Brain Struct Funct
DOI 10.1007/s00429-013-0641-4

ORIGINAL ARTICLE

Multivariate classification of social anxiety disorder using whole brain functional connectivity

Feng Liu · Wenbin Guo · Jean-Paul Fouche · Yifeng Wang · Wenqin Wang · Jurong Ding · Ling Zeng · Changjian Qiu · Qiyong Gong · Wei Zhang · Huafu Chen

Received: 30 April 2013 / Accepted: 12 September 2013

Abstract Recent research has shown that social anxiety disorder (SAD) is accompanied by abnormalities in brain functional connections. However, these findings are based on group comparisons, and, therefore, little is known about whether functional connections could be used in the diagnosis of an individual patient with SAD. Here, we explored the potential of the functional connectivity to be used for SAD diagnosis. Twenty patients with SAD and 20 healthy controls were scanned using resting-state functional magnetic resonance imaging. The whole brain was divided into 116 regions based on automated anatomical labeling atlas. The functional connectivity between each pair of regions was computed using Pearson's correlation coefficient and used as classification feature. Multivariate pattern analysis was then used to classify patients from healthy controls. The pattern classifier was designed using linear support vector machine. Experimental results showed a correct classification rate of 82.5 % ($p < 0.001$) with sensitivity of 85.0 % and specificity of 80.0 %, using a leave-one-out cross-validation method. It was found that the consensus connections used to distinguish SAD were largely located within or across the default mode network, visual network, sensory-motor network, affective network, and cerebellar regions. Specifically, the right orbitofrontal region exhibited the highest weight in classification. The current study demonstrated that functional connectivity had good diagnostic potential for SAD, thus providing evidence for the possible use of whole brain functional connectivity as a complementary tool in clinical diagnosis. In addition, this study confirmed previous work and described novel pathophysiological mechanisms of SAD.

Electronic supplementary material The online version of this article (doi:10.1007/s00429-013-0641-4) contains supplementary material, which is available to authorized users.

F. Liu · Y. Wang · J. Ding · L. Zeng · H. Chen (✉)
Key Laboratory for NeuroInformation of Ministry of Education, School of Life Science and Technology, University of Electronic Science and Technology of China, Chengdu 610054, Sichuan, People's Republic of China
e-mail: chenhf@uestc.edu.cn

W. Guo
Mental Health Center, The First Affiliated Hospital, Guangxi Medical University, Nanning 530021, Guangxi, People's Republic of China

J.-P. Fouche
Department of Psychiatry, University of Cape Town, Cape Town, South Africa

J.-P. Fouche
Department of Human Biology, University of Cape Town, Cape Town, South Africa

J.-P. Fouche
Department of Psychiatry, University of Stellenbosch, Cape Town, South Africa

W. Wang
School of Mathematical Sciences, University of Electronic Science and Technology of China, Chengdu 611731, Sichuan, People's Republic of China

C. Qiu · W. Zhang
Department of Psychiatry, West China Hospital of Sichuan University, Chengdu 610041, People's Republic of China

Q. Gong
Department of Radiology, Huaxi MR Research Center (HMRRC), West China Hospital of Sichuan University, Chengdu 610041, People's Republic of China

Published online: 27 September 2013

Keywords Social anxiety disorder/social phobia · Multivariate pattern analysis · Support vector machine · Functional connectivity · Resting-state fMRI · Consensus features

Introduction

Anxiety disorders, classified by the Diagnostic and Statistical Manual of Mental Disorders IV (DSM-IV) (APA 1994), are among the most common psychiatry disorders. Even so, social anxiety disorder (SAD), one of the most common anxiety disorders (Fink et al. 2009; Fouche et al. 2013; Jefferys 1997), has received relatively little attention. SAD, also termed social phobia (Stein and Stein 2008), is characterized by an excessive and unreasonable fear of social interactions and performance situations wherein the individual fears negative evaluation by others. Patients with SAD typically avoid the feared situations or endure them with intense feelings of anxiety or distress, thus leading to significant functional impairment (Talati et al. 2013). Epidemiological research conducted on the general population has demonstrated that the lifetime prevalence of SAD ranges between 4 and 16 % (Ohayon and Schatzberg 2010). At present, however, SAD is diagnosed mainly based on clinical signs and symptoms, and its pathophysiology remains largely unclear. Undoubtedly, it is important to explore a valid and objective biomarker to distinguish patients with SAD from healthy controls.

In recent years, resting-state functional magnetic resonance imaging (fMRI) has attracted considerable attention. This technique not only overcomes potential limitations associated with task paradigms in fMRI studies but is also relatively easy and more economical to implement than positron emission tomography (PET) and single photon emission computed tomography (SPECT) in clinical studies (Greicius 2008). Moreover, resting-state fMRI is a novel non-invasive imaging technique for measuring spontaneous brain activity as low-frequency fluctuations in blood oxygen level–dependent (BOLD) signals to identify areas of increased or decreased neuronal activity (Biswal et al. 1995; Fox and Greicius 2010; Guo et al. 2011; Liu et al. 2012b). Resting-state functional connectivity has been defined as the identification of correlation patterns between these fluctuations measured in different brain areas and has the potential to greatly increase the translation of fMRI into clinical care (Fox and Greicius 2010). By using resting-state functional connectivity, previous studies focused on the quantitative analysis of the brains in patients with psychiatric and neurological diseases, such as major depression (Guo et al. 2013), Alzheimer's disease (Zhou et al. 2013), and schizophrenia (Liu et al. 2008). In addition, a recent study found decreased functional connectivity of the left amygdala with the medial orbitofrontal cortex and the posterior cingulate gyrus (PCG)/precuneus (PCUN) in SAD (Hahn et al. 2011). However, little is known about whether the altered functional connectivity could be used in the diagnosis of an individual patient with SAD. For clinical purposes, one must be able to provide predictions at the level of the individual patient (Smith 2012).

As a data-driven technique, multivariate pattern analysis (MVPA) plays an important role in analyzing neuroimaging data. In contrast to conventional approaches that are mainly based on univariate and group-level statistical methods, MVPA method is sensitive to the fine-grained spatial discriminative patterns and exploration of inherent multivariate nature from high-dimensional neuroimaging data (Norman et al. 2006). Furthermore, MVPA could provide novel insight into the differences between two groups because it allows the identification of features which contribute the most to individual classification (Meier et al. 2012). Recently, an increasing number of neuroimaging studies focused on applying MVPA to discriminate psychiatric patients from healthy controls (Anderson et al. 2011; Liu et al. 2012a; Uddin et al. 2011).

To date, no MVPA studies have been published on patients with SAD. Such studies are particularly important, because it can examine whether MVPA and functional connectivity could become a clinical tool for the diagnosis of SAD, with emphasis on early treatment. In the present study, our goal was to determine whether MVPA and whole brain resting-state functional connectivity could help to discriminate, at an individual level, patients with SAD from healthy controls. Specifically, a pattern classifier was designed using linear support vector machine (SVM) to perform classification between the patient and control groups and to identify functional connections with distinct characteristics. Previous findings have revealed functional connectivity differences between patients and controls. Therefore, we hypothesized that functional connectivity could be used as a potential biomarker to distinguish patients from controls. Additionally, we also hypothesized that aberrant functional connections would be observed in the resting-state networks involved in social cognition and emotional processing. We hoped that by thoroughly exploring the whole brain we could finally obtain additional information for advancing our understanding of the pathophysiology of this disorder.

Materials and methods

Subjects

The present study was approved by the Ethics Committee of the Huaxi Hospital, Sichuan University, Chengdu,

China. Written informed consent was obtained from each participant before any study procedure was initiated. Twenty-three patients with SAD were recruited from Mental Health Center of the Huaxi Hospital. All patients did not receive psychiatric and psychotherapy medications. SAD was diagnosed by two attending psychiatrists and a trained interviewer using the Structured Clinical Interview DSM-IV (SCID) Patients Version. Exclusion criteria included participants with ages younger than 18 or older than 40 years, any history of major physical illness, cardiovascular disease, bipolar disorder, neurological illness, or a lifetime history of alcohol or drug use. Twenty age-, sex-, and education-matched healthy controls were recruited from the local community by advertisements. The same psychiatrists and interviewer that used the SCID Non-Patient Version to confirm the current absence of psychiatric and neurological illness screened them as well. None of them had any neurological or psychiatric disorders. There was also no major psychiatric or neurological illness among their first-degree relatives.

All participants were evaluated with the State-Trait Anxiety Inventory (STAI), Hamilton Anxiety Rating Scale (HAMA), Hamilton Depression Rating Scale (HAMD), and Liebowitz Social Anxiety Scale (LSAS). Specifically, the STAI questionnaire consists of two parts: the STAI-State (STAI-S) score, which gives the level of state anxiety at the time of completing the text, and the STAI-Trait (STAI-T) score, which gives the level of inherent trait anxiety of the subject. The STAI-S questionnaire was completed before and after the MRI scanning (pre-scanning and post-scanning) session (Campbell et al. 2007).

Data acquisition

The MR images were acquired on the 3.0-T GE-Signa MRI scanner (Excite, General Electric, Milwaukee, USA) in Huaxi MR Research Center, Chengdu, China. Foam padding was used to minimize head movement. During data acquisition, the participants were instructed to hold still, relax minds, and move as little as possible. Functional images were performed by a single-shot, gradient-recalled echo-planar imaging (EPI) sequence. Sequence parameters were as follows: repetition time/echo time (TR/TE) = 2,000/30 ms, thickness = 5 mm, no slice gap, field of view (FOV) = 24 cm, flip angle (FA) = 90°, data matrix = 64 × 64, voxel size = 3.75 × 3.75 × 5 mm^3. Five dummy scans were discarded to remove the impact of magnetization instability. For each participant, the brain volume comprised 30 axial slices, and each functional run contained 200 image volumes.

Data preprocessing

Image preprocessing was carried out using the statistical parametric mapping (SPM8, http://www.fil.ion.ucl.ac.uk/spm) software package. For each participant, EPI images were first corrected for the temporal differences between slices and then realigned to correct head motion. Recent studies demonstrated that head motion had a substantial impact on resting-state functional connectivity (Power et al. 2012; Satterthwaite et al. 2012; Van Dijk et al. 2012). Thus, only participants with head motion less than 2.0 mm in the *x*, *y,* or *z* direction and less than 2.0° rotation in each axis were included. Besides, "Mean motion" was computed and compared between the subject groups to further determine the comparability of head movement across groups, as suggested by Van Dijk et al. (2012). Then, the corrected images were spatially normalized to the Montreal Neurological Institute (MNI) EPI template in SPM8 and resampled to 3 mm cubic voxels. In order to avoid introducing artificial local spatial correlations, no spatial smoothing was applied, as previously suggested (Achard et al. 2006; Wang et al. 2009; Zhang et al. 2011b, c).

Anatomical parcellation

The registered fMRI data were further divided into 116 anatomical regions of interests (ROIs) according to the automated anatomical labeling (AAL) atlas (Tzourio-Mazoyer et al. 2002), which was shown in Figure S1 in Supplement 1. This atlas parcellates the brain into 78 cortical regions (39 in each hemisphere), 12 subcortical regions (6 in each hemisphere), and 26 cerebellar regions (9 in each cerebellar hemisphere and 8 in the vermis). Details of AAL regions can be found in Table S1 in Supplement 1. From a network perspective, these regions belong to several different resting-state networks, such as default mode network (DMN), visual network (VN), sensory-motor network (SMN), and affective network (AN). For the details of the regions in these resting-state networks, see Supplement 1.

Functional connectivity of the whole brain

For each subject, a representative time series in each region was obtained by averaging the fMRI time series of all voxels in each of the 116 regions (Liu et al. 2007; Yu et al. 2008). These representative time series were temporally band-pass filtered (0.01–0.08 Hz) to reduce the effects of low-frequency drift and high-frequency physiological noises (Liao et al. 2010b). Several sources of spurious variance were removed by regression along with their first derivatives: six head motion parameters obtained by rigid body correction, signal from a region centered in the white

matter and signal from a ventricular region of interest. This regression procedure removed variances unlikely to be involved in specific regional correlations of neuronal origin (Fox et al. 2005). Of note, it is still an ongoing controversy of removing the global signal in the preprocessing of resting-state fMRI data (Fox et al. 2009; Murphy et al. 2009; Saad et al. 2012). Therefore, we did not regress out the global signal. The residuals of these regressions were used for the following functional connectivity analysis. Functional connectivity between each pair of regions was evaluated using Pearson's correlation coefficients, resulting in $(116 \times 115)/2 = 6{,}670$ dimensional functional connectivity feature vectors for each subject. These functional connections were the features used in all subsequent analyses.

Feature selection

Given that some features are uninformative, irrelevant or redundant for classification, reducing a number of features not only speed up computation, but also improve classification performance (Dosenbach et al. 2010; Pereira et al. 2009). Therefore, an initial feature selection step was utilized. In this study, the F score method was employed for feature ranking (Chen and Lin 2006). F score is simple, generally quite effective, and used in previous studies (Akay 2009; Huang et al. 2007).

Given the number of positive instances (i.e., patient subjects) n_+ and negative instances (i.e., control subjects) n_-, the F score of the ith feature is defined as follows (Chen and Lin 2006):

$$F(i) = \frac{\left(\bar{x}_i^{(+)} - \bar{x}_i\right)^2 + \left(\bar{x}_i^{(-)} - \bar{x}_i\right)^2}{\frac{1}{n_+ - 1}\sum_{k=1}^{n_+}\left(x_{k,i}^{(+)} - \bar{x}_i^{(+)}\right)^2 + \frac{1}{n_- - 1}\sum_{k=1}^{n_-}\left(x_{k,i}^{(-)} - \bar{x}_i^{(-)}\right)^2}, \quad (1)$$

where $\bar{x}_i$, $\bar{x}_i^{(+)}$, $\bar{x}_i^{(-)}$ are the averages of the ith feature of the whole, positive, and negative data sets, respectively; $x_{k,i}^{(+)}$ is the ith feature of the kth positive instance, and $x_{k,i}^{(-)}$ is the ith feature of the kth negative instance. The denominator represents the discrimination within each of the positive and negative sets, while the numerator represents the discrimination between the two sets. Obviously, the larger the F score is, the more discriminative the feature is.

A leave-one-out cross-validation (LOOCV) strategy was used to evaluate the performance of a classifier (see immediately below). For each LOOCV fold, we ranked the features according to their F scores in descending order and retained the 250 highest ranked features (see details in the following subsection of "Overall classifier performance"). It was worth noting that all the procedures of feature selection were constrained in the training set of each LOOCV fold, without using the information of the testing set, in order to avoid the introduction of bias.

Since feature ranking was based on a slightly different subset of the data in each iteration of LOOCV, the final features (in our case functional connections) used in classification differed for each iteration of LOOCV. Consensus features were introduced here. They were defined as the common features always selected to form the final feature set from each LOOCV iteration. Feature weights (i.e., support vector classification weights) of the consensus functional connections were the average across all folds of LOOCV. To represent the relative contribution of different regions for classification, the weight of each region to the overall ability of the classifier to accurately discriminate between two groups could be evaluated by summing one-half of the consensus feature weights associated with that region (Meier et al. 2012). Of note, if a region did not form any consensus functional connections, it was given a region weight of zero.

Classification and support vector machine

Support vector machine (SVM) classifier was adopted here for classification. This technique works well when the number of training samples is small but the number of features is large (Vapnik 1995). SVM classification is a form of supervised learning because training is accomplished by labeled samples (Burges 1998). A binary label with 1 for patients and -1 for healthy controls was used here. The classification process consists of two steps: training and testing. During the training step, the SVM finds a decision boundary that separates the examples in the input space using their class labels. Once the decision function is determined from the training set, it can be used to predict the class label of a new testing example.

A linear kernel SVM was used to reduce the risk of overfitting the data and to allow direct extraction of the feature weights (Pereira et al. 2009). The linear SVM has only one parameter C that determines the trade-off between allowing misclassifications and training error minimization. The SVM classifier was implemented using LIBSVM toolbox (Chang and Lin 2011), with a default value for the parameter C (i.e., $C = 1$).

Evaluation on the performance of Classifier

Due to our limited number of samples, a LOOCV strategy was employed to evaluate the performance of the classifier (Schölkopf et al. 2001; Wee et al. 2011). In brief, suppose there were n samples in total. In each LOOCV trial, we used $n-1$ samples as the training set and the remaining one was used as the testing set. Classifiers were built for each

training set and tested with its corresponding testing subject. Accuracy, sensitivity, and specificity could be used to quantify the performance of the classifier based on the results of LOOCV.

$$\text{Accuracy} = \frac{\text{TP} + \text{TN}}{\text{TP} + \text{FN} + \text{TN} + \text{FP}} \quad (2)$$

$$\text{Sensitivity} = \frac{\text{TP}}{\text{TP} + \text{FN}} \quad (3)$$

$$\text{Specificity} = \frac{\text{TN}}{\text{TN} + \text{FP}}, \quad (4)$$

where TP is the number of true positives: number of patients correctly classified; TN is the number of true negatives: number of normal controls correctly classified; FP is the number of false positives: number of normal controls classified as patients; FN is the number of false negatives: number of patients classified as normal controls.

To assess whether the computed classification accuracy is statistically significant, the statistical significance of the classification results is evaluated using permutation test as proposed by Golland and Fischl (2003). The permutation test is a non-parametric technique which is used to test the null hypothesis that the computed accuracy is obtained by chance (Mourao-Miranda et al. 2005; Wang et al. 2012; Zhu et al. 2008). In the permutation test, the class labels of the original data S are randomly permuted to obtain a set of k randomized versions of data, $\hat{S} = \{S'_1, S'_2, \ldots, S'_k\}$. A classifier is then built based on each of the S' and test on the same testing data. The p value of the permutation test is defined as the fraction of the number of classifiers that built based on S' which is better than the classifier that built based on S, which is given as

$$p = \frac{\left|\{S' \in \hat{S} : \text{acc}(S') \geq \text{acc}(S)\}\right| + 1}{k + 1}, \quad (5)$$

where $\text{acc}(S)$ represents the accuracy obtained from the original data S and $\text{acc}(S')$ represents the accuracy obtained from the randomized data S'. The p value of Eq. (5) measures how likely the observed accuracy is obtained by chance. The smaller the p value is, the more unlikely it is obtained by chance, and the more reasonable we reject the null hypothesis. In the current analysis, the class labels (i.e., SAD vs. healthy controls) of the training data were permuted 1,000 times at random prior to training and then the same entire classification process including feature selection was carried out with each set of permuted class labels. The accuracies were obtained across all permutations and the p value was calculated as the proportion of accuracies that are equal to or greater than the accuracy obtained by the non-permutated (original) data. If less than 5 % ($p < 0.05$) of the accuracies from all permutations exceeded the non-permutated value, the result was thought to be significant.

Results

Demographics and clinical characteristics of the participants

Data of three patients with SAD were excluded because translation and rotation exceeded ±2 mm or ±2°. Two-sample t tests were performed to assess the differences in age, years of education, head movement, and clinical scores, while Chi-square test was performed to assess the difference in gender. The two groups were matched for gender (14 males for SAD group and 14 males for control group), age (22.90 ± 3.99 years for SAD group; 21.75 ± 3.73 years for healthy controls; $p = 0.313$), years of education (14.10 ± 1.48 years for SAD group; 14.05 ± 1.96 years for healthy controls; $p = 0.928$), and the head motion (0.034 ± 0.012 mm for SAD group; 0.040 ± 0.020 mm for healthy controls; $p = 0.258$). Relative to healthy controls, patients with SAD have significantly higher scores of LSAS, HAMD, HAMA, and significantly higher levels of anxiety assessed by the STAI-T and pre-scanning STAI-S. The detailed demographic and clinical data are presented in Table 1.

Table 1 Demographics and clinical characteristics of patients with SAD and HC

Variables (Mean ± SD)	SAD	HC	p value
Gender (M/F)	20 (14/6)	20 (14/6)	–
Age (years)	22.90 ± 3.99	21.75 ± 3.73	0.313
Education (years)	14.10 ± 1.48	14.05 ± 1.96	0.928
Illness duration, (months)	45.40 ± 39.78	–	–
LSAS			
Total score	53.90 ± 11.50	20.00 ± 8.27	<0.001
Fear factor	28.00 ± 6.17	8.40 ± 4.81	<0.001
Avoidance factor	25.90 ± 6.93	11.60 ± 5.91	<0.001
HAMD	7.50 ± 6.27	1.30 ± 1.87	<0.001
HAMA	6.20 ± 4.74	1.22 ± 1.80	<0.001
STAI			
STAI-T	48.25 ± 7.02	32.90 ± 4.93	<0.001
STAI-S			
Pre-scanning	41.35 ± 8.31	31.40 ± 4.85	<0.001
Post-scanning	37.65 ± 9.54	33.10 ± 7.08	0.095
Head motion	0.034 ± 0.012	0.040 ± 0.020	0.258

SAD social anxiety disorder, *HC* healthy controls, *LSAS* Liebowitz Social Anxiety Scale, *HAMA* Hamilton Anxiety Rating Scale, *HAMD* Hamilton Depression Rating Scale, *STAI* State-Trait Anxiety Inventory

The p values were obtained by two-sample t test

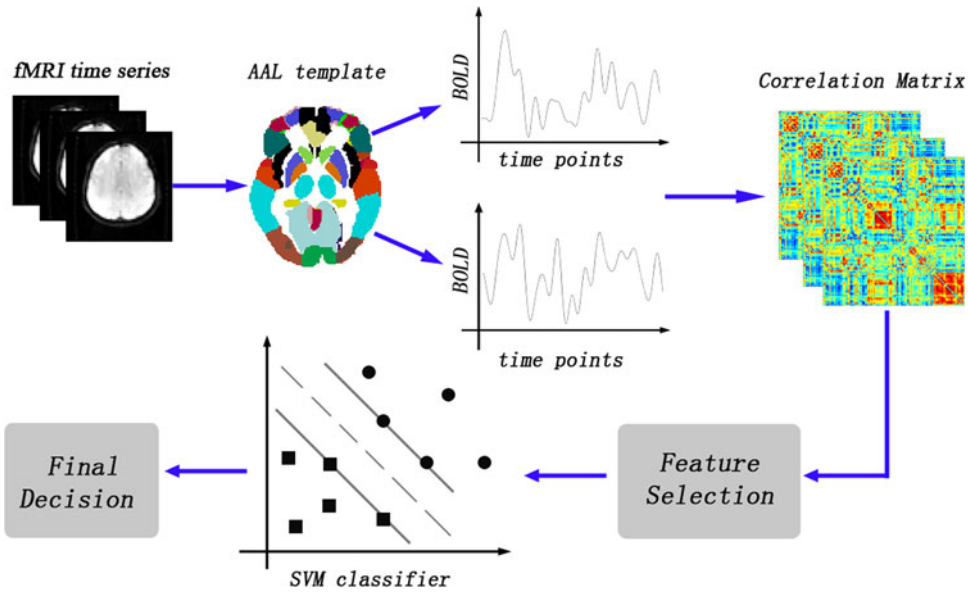

Fig. 1 Schematic diagram illustrating the proposed classification framework

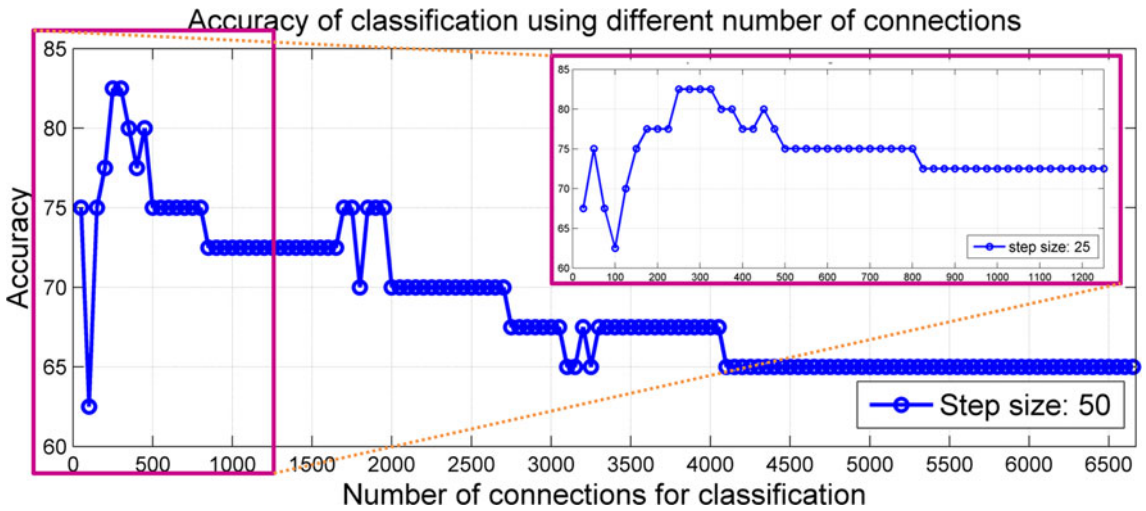

Fig. 2 Predictive accuracy as a function of the number of connections used in the classification process. The connections were ranked according to F scores in descending order

Overall classifier performance

An overview of the proposed MVPA framework was summarized in Fig. 1. As shown in Fig. 2, the linear SVM classifier could reach up to 82.5 % (85 % for sensitivity, 80 % for specificity, $p < 0.001$) by using the 250 highest ranked functional connections. Thus, we selected the top 250 ranked features in each iteration of LOOCV for the classification features. In addition, the discriminative score of each testing subject was acquired by the SVM classifier. Taking each subject's discriminative score as a threshold, the receiver operating characteristic (ROC) curve of the classifier was yielded, as shown in Fig. 3. The area under the ROC curve (AUC) of the proposed method was 0.852, indicating a good classification power.

Consensus features

In this study, 148 features, known as consensus features, were identified in the cross-validation. The consensus functional connections were mainly located within or across the DMN, VN, SMN, AN, and cerebellum. The consensus functional connections related to these networks are shown in Fig. 4.

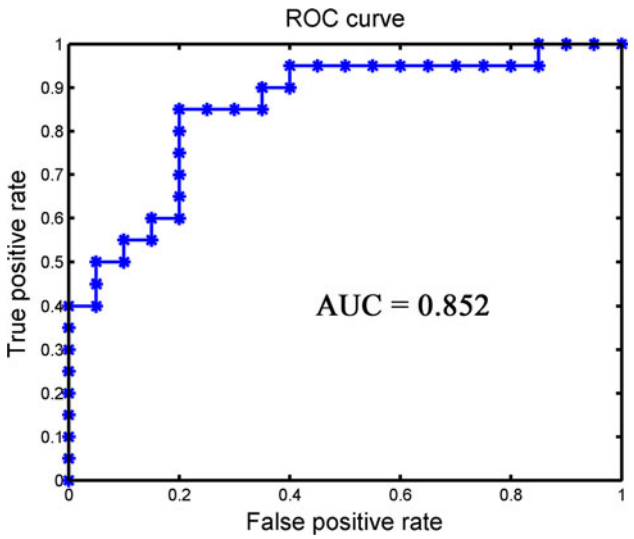

Fig. 3 ROC curve of the classifier. *ROC* receiver operating characteristic

Region weight

Some regions showed greater weights than others. Specifically, we defined a region having significantly higher weight if its weight was at least one standard deviation greater than the average of the weight of all the regions, as used in a previous study (Tian et al. 2011). The regions with the greater weight included the right orbital part of the middle frontal gyrus (MFGorb), the left PCUN, the left lingual gyrus (LING), the right orbital part of the superior frontal gyrus (SFGorb), the right insula (INS), the left postcentral gyrus (PoCG), the left middle part of temporal pole (TPOmid), the left superior occipital gyrus (SOG), the right superior part of temporal pole (TPOsup), the vermis_1&2 (VER 1&2), and the left angular gyrus (ANG). Figure 5 displays these regions.

Comparison between linear and non-linear SVM classifiers

Non-linear SVM classifier (i.e., radial basis function (RBF) kernel SVM) was trained and tested with the same procedure used in the proposed framework to validate the effectiveness of using linear SVM classifier. For fair comparison, default parameters were used for both linear and non-linear SVM classifiers. Figure 6 shows that non-linear SVM classifier achieves the best accuracy of 75 % when the 250 highest ranked functional connections are used. Results in Table 2; Fig. 7 show that linear SVM classifier performs better than non-linear SVM classifier in terms of accuracy, sensitivity, specificity, and AUC value.

Comparison between linear SVM classifier and *k*-nearest neighbors (*k*-NN) classifier

To further understand the performance of the linear SVM classifier, we applied *k*-NN classifier to the same data. In the machine learning field, *k*-NN method is a non-parametric lazy learning algorithm for classifying testing samples on the basis of the closest training samples in the feature space (Cover and Hart 1967). In addition, *k*-NN method is one of the simplest machine learning algorithms. This method entailed finding the k nearest neighbors and performing a majority voting of its neighbors. The main advantage of *k*-NN classifier is that it is more intuitive than SVM and less labor-intensive because no parameter is required except k (i.e., the number of neighbors). In the current study, *k*-NN was used with the same training and testing procedure in the proposed framework by utilizing the MATLAB R2012a (Mathworks, Natick, Massachusetts) "ClassificationKNN.fit" and "predict" functions. As seen in Table 3, linear SVM classifier outperformed *k*-NN classifier in SAD classification. Specifically, with default parameter ($k = 1$), the *k*-NN (i.e., nearest neighbor algorithm) classifier achieved accuracy of 72.5 % (when we used the 850 highest ranked functional connections), with a sensitivity of 75.0 %, and a specificity of 70.0 %. We also performed grid search to determine the best number of neighbors (k) for *k*-NN classifier. It is found that *k*-NN classifier achieves the highest accuracy of 80.0 % when $k = 3$ and when 300 highest ranked functional connections are used, as shown in Fig. 6.

Discussion

To the best of our knowledge, the current study is the first to apply MVPA to discriminate patients with SAD from healthy controls. Our study had three main findings: (1) a promising classification performance had been validated by LOOCV: our method achieved a relatively high accuracy (82.5 %) for SAD classification and the AUC value was 0.852, indicating good potential for diagnosis; (2) most of the consensus functional connections were located within or across the DMN, VN, SMN, AN, and cerebellum; (3) the region of the right MFGorb exhibited the highest weight in classification.

Our findings showed that the altered functional connections were related to the DMN. The DMN is thought to be a higher-level cognitive network system and comprises a set of brain regions that typically deactivate during performance of goal-directed tasks and activate during resting state (Raichle et al. 2001). The main function of the DMN is self-referential activity, which is impaired in SAD (Anderson et al. 2008). Abnormality of the DMN in SAD

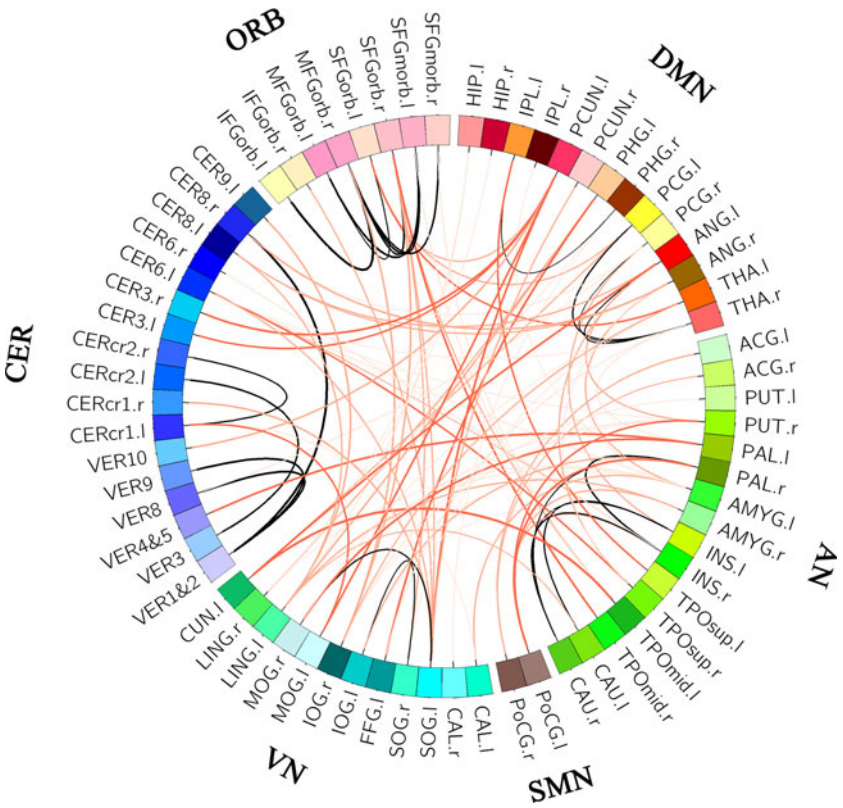

Fig. 4 This is a connectogram that shows the consensus functional connections within or across the default mode network, visual network, sensory-motor network, affective network, orbitalfrontal cortex and cerebellum. The brain region of each cluster is represented by a *square* on the circumference of the big circle. The *lines* connecting two squares represent the connections between the corresponding two brain regions. The thickness of the line represents the weight (i.e., support vector classification weight) of the connection. The thicker the line, the larger the weight. The *red lines* represent inter-network connections and the *black lines* represent intra-network connections. *DMN* default mode network, *AN* affective network, *SMN* sensory-motor network, *VN* visual network, *CER* cerebellum, *ORB* orbitalfrontal cortex. This visualization was created using Circos (http://circos.ca/)

has been found in previous studies (Gentili et al. 2009; Liao et al. 2010a). Thus, our results supported the notion that DMN played a key role in SAD. Moreover, the left PCUN and the left ANG were shown to have high weights. The PCG/PCUN is not only the critical hub of the DMN involved in social cognition (Gentili et al. 2009; Raichle et al. 2001), but also a core hub of the whole brain network (Hagmann et al. 2008). Patients with SAD showed a lower deactivation in the PCG/PCUN regions during task conditions (Gentili et al. 2009). In addition, Warwick and colleagues found a decreased perfusion of the PCUN in patients with SAD during resting state, indicating that the abnormal functional connectivity in PCUN may be linked with the pathophysiological mechanism underlying SAD (Warwick et al. 2008). The ANG, another hub of DMN, plays a critical role in mental constructs such as thoughts, feelings, and beliefs (Frith and Frith 2003). A recent task-based study reported that the ANG had a greater BOLD response when patients reacted to feelings of negative self-belief (Goldin and Gross 2010). Accumulated evidence demonstrated that SAD was characterized by emotional biases and distorted negative self-beliefs (Goldin et al. 2009a). Furthermore, Qiu et al. (2011) found a decreased regional homogeneity in bilateral ANG. Thus, our finding was consistent with previous studies and suggested that the connections related to the ANG were abnormal in the resting state.

In addition to the DMN, perceptual networks were shown to be altered in SAD. In contrast to DMN, the perceptual networks can be considered as lower-level cognitive processing. Commonly, the perceptual networks include the VN, SMN and auditory network. Aberrant functional connectivity and high region weight were found in the visual processing network (LING and SOG) and sensory processing network (PoCG), which might contribute to perceptual impairments in SAD. To some extent, this result was in line with previous findings. For example, greater activity was found after treatment in SMN and VN in a social anxiety imagery task (Kilts et al. 2006). Using a social (harsh facial expressions) and physical (violent scenes) threat task, Goldin et al. (2009b) found significantly greater BOLD responses in SAD. Furthermore, a

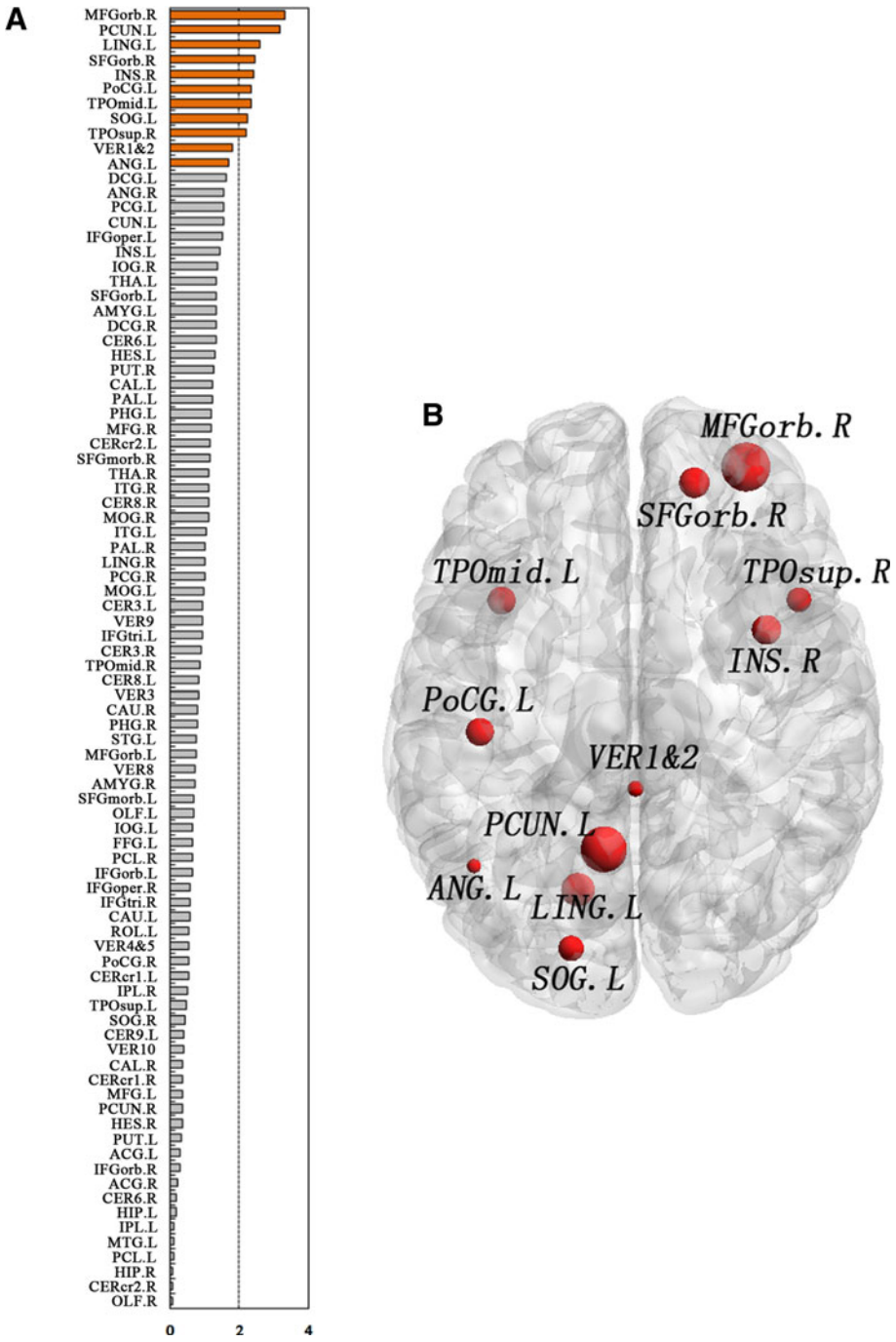

Fig. 5 The region weight in the classification. **a** Bar plot of the values of mean normalized region weight for the detected brain regions that related to consensus functional connections in descending order. The regions with *orange color* represent the regions having significantly higher weight. **b** Rendering plot of the regions with significantly higher weight in the classification. The size of the node represented the magnitude of the normalized region weight. *L* left, *R* right

pilot structural MRI study showed that patients with SAD had significant bilateral cortical thinning in the visual and sensory regions (Syal et al. 2012). Taken together, these findings indicated that the altered perceptual networks might be related to impaired visual and sensory function in SAD.

The AN, which is involved in emotional processing (Mayberg et al. 1999), is important to fear, vigilance and visceral regulation (Olson et al. 2007). The INS and temporal pole (TPO) were found to exhibit the high weights. The INS has increasingly become the focus of attention for its role in body representation and subjective emotional experience. Recently, Borg et al. (2012) found impaired emotional processing in patients with an INS lesion. Some evidence further emphasized hyperactivity of the INS of anxiety patients during the processing of negative emotion (Etkin and Wager 2007; Gentili et al. 2008). We speculated that functional abnormality of the INS

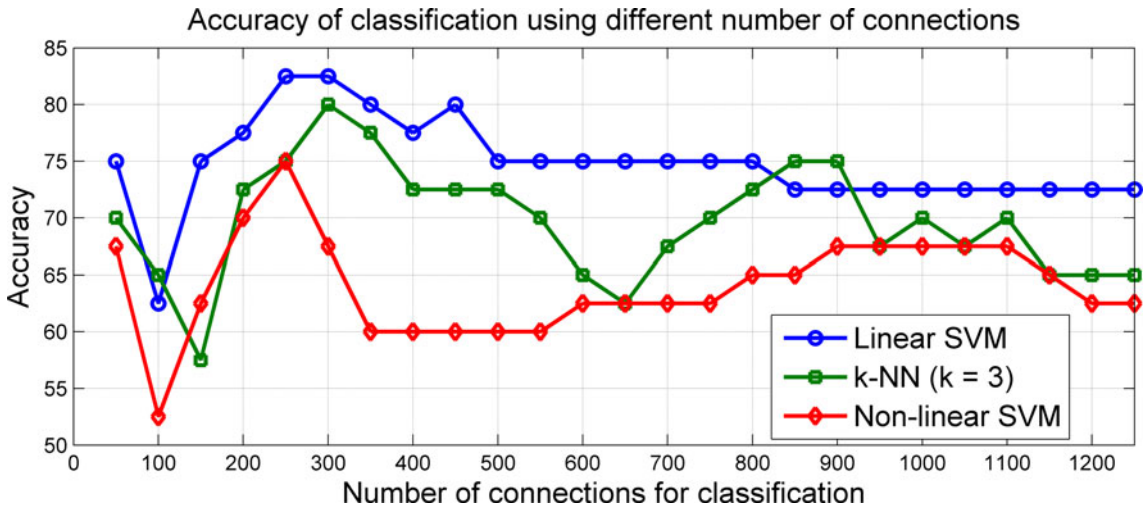

Fig. 6 Predictive accuracy as a function of the number of connections used in the classification process by using linear SVM, non-linear SVM and *k*-NN classifiers. The connections were ranked according to *F* scores in descending order

Table 2 Classification performance for linear and non-linear SVM classifiers

SVM classifier	Accuracy	Sensitivity	Specificity	AUC
Non-linear (RBF)	75.0	75.0	75.0	0.805
Linear	82.5	85.0	80.0	0.852

RBF radial basis function

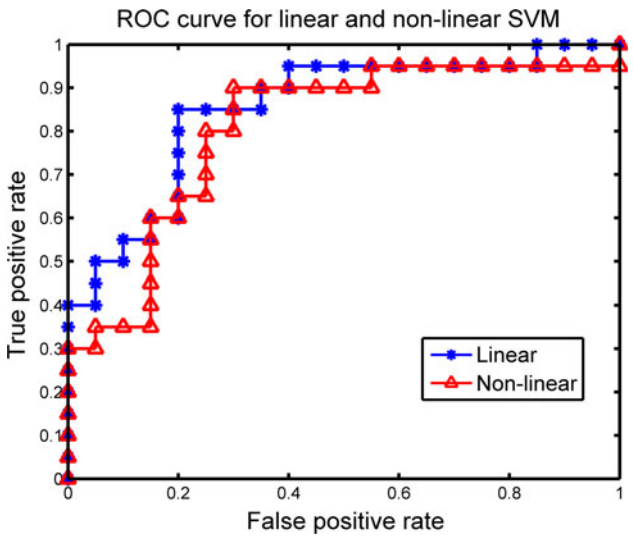

Fig. 7 ROC curves of the linear and non-linear SVM classifier. In this study, non-linear SVM denotes the RBF kernel SVM

would disrupt functional connectivity from INS to other brain systems. Additionally, the TPO region plays an important role in social and emotional processing as a paralimbic region (see the review by Olson et al. (2007)). Moreover, previous study in healthy subjects found

Table 3 Classification performance for linear SVM and *k*-NN classifiers

Method	Accuracy	Sensitivity	Specificity
k-NN ($k = 1$, default parameter)	72.5	75.0	70.0
k-NN ($k = 3$, best parameter)	80.0	85.0	75.0
Linear SVM	82.5	85.0	80.0

k-NN *k*-nearest neighbors

activation in this region during social perception and competition with the mental states of others (Polosan et al. 2011). In contrast, impairment in TPO led to alterations in the ability to characterize social attributes of behavior (Zahn et al. 2007). Tillfors et al. demonstrated that decreased blood flow of the TPO was found during anticipation of public speaking (Tillfors et al. 2002) and stressful speaking tasks (Tillfors et al. 2001). The above-mentioned indicate that altered functional connections in AN may lead to poor emotion regulation which is found in patients with SAD.

It was unexpected that the cerebellar region had relatively high weight. Up to now, a large number of neuroimaging studies have focused on the cerebral cortex in SAD, not really considering the role of the cerebellum in this disorder. The traditional view on cerebellum function is on the acquisition of motor coordination and motor behavior (Stein and Glickstein 1992). However, a recent study found that the cerebellum was involved in emotional control and played a role in the perception of emotional stimuli (Schmahmann 2010). Moreover, both structural and functional studies found changes in the cerebellum in SAD. Warwick et al. (2008) demonstrated both hyper- and

hypo-perfusion in the cerebellum among patients with SAD, and a social situation task-based fMRI study reported significantly decreased activation in the cerebellum (Nakao et al. 2011). In addition, Kilts and colleagues found that inducing anxiety in patients with SAD increased blood flow to the cerebellum (Kilts et al. 2006). Furthermore, patients with SAD had greater gray matter volume in the cerebellum compared with healthy controls (Talati et al. 2013). In spite of the fact that the mechanisms are remaining largely unknown, cerebellar abnormalities may increase vulnerability to anxiety states via modulation of arousal. Many cerebellar subdivisions and the vermis in particular project to the fastigial nucleus and then to the pons and medulla oblongata, which mediate the autonomic responses that are exaggerated in subjects with anxiety (Baldacara et al. 2008). Overall, these findings may provide a basis for the cerebellar regions to participate in emotional processing.

The region of right MFGorb had the highest weight. As shown in literature, SAD is characterized by a hyper-activated right prefrontal cortex (Engel et al. 2009). A previous study demonstrated that a lesion in the orbitofrontal cortex would impair self-insight, which might preclude the generation of helpful emotional information (Beer et al. 2006). According to the orbitofrontal cortex-anger hypothesis, this region is also the core hub of angry emotion [see the review by Lindquist et al. (2012)]. In addition, the orbitofrontal cortex assigns positive and negative stimulus response contingencies and regulates expression of emotion (Blackmon et al. 2011; Milad and Rauch 2007). Taken together, altered functional connectivity associated with the orbitofrontal region may contribute to emotional dysregulation exhibited by SAD.

From a local scale viewpoint, the brain is organized into multiple resting-state networks (Damoiseaux et al. 2006; Sorg et al. 2007) as mentioned above. From a global scale viewpoint, the human brain is a complex network which continuously integrates information across different brain networks (Bullmore and Sporns 2012; Jiang 2013). In addition to the aberrant intra-network connectivity, we also found altered inter-network connectivity. Investigation of the intra-network connectivity may advance our understanding of the functional specialization of the brain, while investigation on inter-network connectivity may increase our understanding of the functional integration within the brain (Friston 2004; Sporns 2011). Inter-network connectivity may provide additional information to understand the pathophysiology underlying the symptoms of SAD. Relative to intra-network connectivity, which is low on the level of the hierarchy, inter-network connectivity is higher in the hierarchy (Luo et al. 2011). Thus, the changed inter-network connectivity might disrupt the high-level complex function which integrates information from multi-networks, such as impression formation and revision (Haker et al. 2013), learning (Gross-Isseroff et al. 2010) and emotion processing (Bruhl et al. 2011, 2013; Hattingh et al. 2012).

MRI-related classification is a challenging task due to the high dimensionality of MRI features but small number of available training samples. The consequence of this is that it is possible to find a decision function which has good classification performance for the samples in the training set, but has poor predictive performance in the testing set: this phenomenon is called overfitting (Mitchell 1997). One way of alleviating the danger of overfitting lies in the choice of the classifier. The advantage of linear SVM is that the model is simple. In addition, it can reduce the risk of overfitting and allow direct extraction of the feature weights. We performed an experiment for comparison between the linear and non-linear SVM classifiers. The results revealed that linear SVM outperformed non-linear SVM for our SAD classification purpose, the rationale for which might be twofold: first, the non-linear SVM may overfit the data in the training set due to the "small sample size, large feature size" problem; second, for fair comparison, we used default parameters in both linear and non-linear SVM classifiers which may degenerate the classification performance of non-linear SVM classifier. We also performed a comparison between the linear SVM and *k*-NN method. As one of the simplest classification methods, nearest-neighbor method does not involve explicit learning of a classification function. Classification of a testing sample is done by finding the most similar training sample and assigning the label of this nearest neighbor to the testing sample. The theory of *k*-NN method (a variant of nearest-neighbor method) is that a testing sample is classified by a majority vote of its *k* neighbors, with the sample being assigned to the label most common amongst its *k* nearest neighbors (*k* is an odd positive integer). The results of Table 3 demonstrate linear SVM classifier performs better than *k*-NN classifier, even though *k*-NN uses the best neighbor size. In addition, we also perform a two-sample *t* test between all the classification accuracies of linear SVM and *k*-NN (i.e., the accuracies corresponding to different number of features). The *p* value obtained is smaller than 0.001, indicating a significant difference between linear SVM and *k*-NN methods. However, we would like to emphasize that the main contribution of this study is to discriminate patients with SAD from healthy controls by using MVPA. Though linear SVM outperforms *k*-NN and non-linear SVM in this study, it is actually based on a small sample size of dataset. In the future, we would like to test our framework using larger dataset to verify whether linear SVM still outperforms other classifiers.

A LOOCV method was used to evaluate the performance of the classifier. Since the selected features for

constructing SVM model were different in each iteration of LOOCV, the SVM models were different across LOOCV folds. Thus, we had forty different SVM models for SAD classification. In the real life application, it would be definitely more suitable to generate only one SVM model, which is used to predict all patients in the future. Ideally, if the sample size was large enough (thousands or tens of thousands of samples), there is no doubt that we can construct a robust and reliable model for predicting new samples. However, in practice, it is too difficult to obtain the MRI data from thousands of patients with SAD and matched healthy controls. For our case, we can use a weighted majority vote strategy to combine different SVM models. Specifically, in the SVM theory, given a new testing sample $\boldsymbol{x}$, the decision function $F_j(\boldsymbol{x})$ of jth linear SVM model for predicted label is

$$D_j(x) = \sum_{i=1}^{n} y_i \alpha_{ij} x_i^T x + b_j \tag{6}$$

$$F_j(x) = \mathrm{sign}\big(D_j(x)\big) \tag{7}$$

where $\boldsymbol{x_i}(i = 1, \ldots, n)$, represents a feature vector of the ith subject and $y_i \in \{1, -1\}$ represents the corresponding class label. α denotes the Lagrange multiplier and b denotes the bias term. Thus, for multiple SVM models, the final decision function $F(\boldsymbol{x})$ of SVM model for predicted label can be written as

$$F(x) = \mathrm{sign}\left(\sum_{j=1}^{m} D_j(x)\right), \tag{8}$$

where m is the total number of SVM models. Using this method, we finally generated one SVM model, which could be utilized to predict new subjects in the future. Alternatively, it *seems* that we can use the consensus features to build a SVM model to test unseen samples. If we used consensus features as final classification features, the two groups could be discriminated with accuracy of 92.5 %. However, this will introduce a bias because of "double dipping" which used the same dataset for selection and analysis (Kriegeskorte et al. 2009). In fact, the consensus features were obtained from all the samples which included training and testing samples. Subsequently, these features were used to build a SVM classifier and LOOCV method was used to evaluate the performance of the classifier. In the feature selection procedure, we cannot include the subjects from testing set. Thus, the result obtained by using consensus features as final classification features did not make sense.

As shown in Fig. 2, the accuracy is 75 % using the 50 highest ranked features. It momentary drops down to 62.5 % using top 100 features, increases back to 75 % using top 150 features, and reaches its maximum at 82.5 % using top 250 features. This looks like a strange phenomenon, but we observe that previous neuroimaging studies have reported similar results as well (Fan et al. 2008; Shi et al. 2007; Su et al. 2012; Tang et al. 2013; Zhang et al. 2011a). The possible reason for this phenomenon may be the fact that, in our study and aforementioned studies, the features are selected based on their rankings of discriminative power which are computed individually and independently. We do not select features based on the discriminative power of the combination of features, as there are too many possible combinations (i.e., 2^{6670}–1). The application of feature selection based on the individual ranking implies that there is no guarantee on the performance of their combinations, e.g., the discriminative power of the combination of the top 100 features might not be better than the combination of the top 50 features for SAD classification. This might be the limitation of this kind of commonly used feature selection method (i.e., select features based on their individual discriminative power rather than select features based on their combination discriminative power). In fact, as shown in Fig. 6, all the comparison methods (non-linear SVM and k-NN) show the similar phenomenon, which indicates that the phenomenon is caused by the feature selection method and not the type of classifier. To overcome this limitation, we will investigate other feature selection methods [e.g., recursive feature elimination (RFE) (Guyon et al. 2002) or sparse representation (Wee et al. 2013)] for SAD classification in the future.

Several limitations should be noted in this study. First of all, our sample size was relatively small. Although the findings were remarkable, the small sample size might limit the translational value of our results. Larger, independent and multi-center imaging datasets will be necessary to confirm our findings. Second, in the current study, the AAL atlas was used to parcellate the whole brain into 116 regions. However, recent studies demonstrated that different parcellation schemes or different spatial scales generated different results (Hayasaka and Laurienti 2010; Wang et al. 2009; Zalesky et al. 2010). Thus, further studies should determine which brain parcellation strategy or spatial scale is more appropriate to discriminate patients with SAD from healthy controls. Third, although we controlled for head motion, we could not fully eliminate this effect. This issue still requires systematic methodological work in the future. Fourth, a total of 250 features were used while we only have 40 subjects; this may lead to the problem of overfitting. However, as described before, linear SVM works well when the number of training samples is small and the number of features is large. Finally, a relatively low sampling rate (TR = 2 s) was used for multislice acquisitions. Under this sampling rate, some inevitable physiological noises, such as respiratory and

cardiac fluctuations of the subject during scanning were reduced but could not be completely removed. Future studies should use a more rigorous approach to correct such physiological noises.

In summary, this study used an MVPA method, which is based on the whole brain resting-state functional connectivity, to distinguish patients with SAD from healthy controls. The current study provided evidence that functional connections have good diagnostic potential. Moreover, the identified altered functional connectivity and high weight regions might provide a complementary method of the clinical diagnosis of SAD. Although functional connectivity was used as feature, the MVPA method is not confined by this kind of feature. Future studies may benefit from the integration of functional connectivity with graph network measures or other imaging modality measurements.

Acknowledgments The authors thank the two anonymous reviewers for constructive suggestions and Kim-Han Thung for the proofreading and valuable comments. H. Chen was supported by the 973 project (No. 2012CB517901), the Natural Science Foundation of China (Nos. 61125304 and 61035006), and the Specialized Research Fund for the Doctoral Program of Higher Education of China (No. 20120185110028). F. Liu was supported by China Scholarship Council (No. 2011607033) and the Scholarship Award for Excellent Doctoral Student granted by Ministry of Education (No. A03003023901010). L. Zeng was supported by the Natural Science Foundation of China (No. 81171406). W. Guo was supported by the Natural Science Foundation of China (Nos. 81260210 and 30900483).

Conflict of interest All authors declare that they have no conflicts of interest.

References

Achard S, Salvador R, Whitcher B, Suckling J, Bullmore E (2006) A resilient, low-frequency, small-world human brain functional network with highly connected association cortical hubs. J Neurosci 26:63–72

Akay MF (2009) Support vector machines combined with feature selection for breast cancer diagnosis. Expert Syst Appl 36:3240–3247

Anderson B, Goldin PR, Kurita K, Gross JJ (2008) Self-representation in social anxiety disorder: linguistic analysis of autobiographical narratives. Behav Res Ther 46:1119–1125

Anderson JS, Nielsen JA, Froehlich AL, DuBray MB, Druzgal TJ, Cariello AN, Cooperrider JR, Zielinski BA, Ravichandran C, Fletcher PT, Alexander AL, Bigler ED, Lange N, Lainhart JE (2011) Functional connectivity magnetic resonance imaging classification of autism. Brain 134:3742–3754

APA. Diagnostic and statistical manual of mental disorders: DSM-*IV*. American Psychiatric Publishing, Inc., 1994

Baldacara L, Borgio JG, Lacerda AL, Jackowski AP (2008) Cerebellum and psychiatric disorders. Rev Bras Psiquiatr 30:281–289

Beer JS, John OP, Scabini D, Knight RT (2006) Orbitofrontal cortex and social behavior: integrating self-monitoring and emotion-cognition interactions. J Cogn Neurosci 18:871–879

Biswal B, Zerrin Yetkin F, Haughton VM, Hyde JS (1995) Functional connectivity in the motor cortex of resting human brain using echo-planar mri. Magn Reson Med 34:537–541

Blackmon K, Barr WB, Carlson C, Devinsky O, Dubois J, Pogash D, Quinn BT, Kuzniecky R, Halgren E, Thesen T (2011) Structural evidence for involvement of a left amygdala-orbitofrontal network in subclinical anxiety. Psychiatry Res 194:296–303

Borg C, Bedoin N, Peyron R, Bogey S, Laurent B, Thomas-Antérion C (2012) Impaired emotional processing in a patient with a left posterior insula-SII lesion. Neurocase. doi:10.1080/13554794.2012.713491

Bruhl AB, Rufer M, Delsignore A, Kaffenberger T, Jancke L, Herwig U (2011) Neural correlates of altered general emotion processing in social anxiety disorder. Brain Res 1378:72–83

Bruhl AB, Herwig U, Delsignore A, Jancke L, Rufer M (2013) General emotion processing in social anxiety disorder: neural issues of cognitive control. Psychiatry Res 212:108–115

Bullmore E, Sporns O (2012) The economy of brain network organization. Nat Rev Neurosci 13:336–349

Burges CJC (1998) A tutorial on support vector machines for pattern recognition. Data Min Knowl Disc 2:121–167

Campbell DW, Sareen J, Paulus MP, Goldin PR, Stein MB, Reiss JP (2007) Time-varying amygdala response to emotional faces in generalized social phobia. Biol Psychiatry 62:455–463

Chang C-C, Lin C-J (2011) LIBSVM: a library for support vector machines. ACM Trans Intell Syst Technol (TIST) 2:27

Chen YW, Lin CJ (2006) Combining SVMs with various feature selection strategies. Feature Extr 207:315–324

Cover T, Hart P (1967) Nearest neighbor pattern classification. IEEE Trans Inform Theory 13:21–27

Damoiseaux JS, Rombouts SA, Barkhof F, Scheltens P, Stam CJ, Smith SM, Beckmann CF (2006) Consistent resting-state networks across healthy subjects. Proc Natl Acad Sci USA 103:13848–13853

Dosenbach NUF, Nardos B, Cohen AL, Fair DA, Power JD, Church JA, Nelson SM, Wig GS, Vogel AC, Lessov-Schlaggar CN (2010) Prediction of individual brain maturity using fMRI. Science 329:1358

Engel K, Bandelow B, Gruber O, Wedekind D (2009) Neuroimaging in anxiety disorders. J Neural Transm 116:703–716

Etkin A, Wager TD (2007) Functional neuroimaging of anxiety: a meta-analysis of emotional processing in PTSD, social anxiety disorder, and specific phobia. Am J Psychiatry 164:1476–1488

Fan Y, Resnick SM, Wu X, Davatzikos C (2008) Structural and functional biomarkers of prodromal Alzheimer's disease: a high-dimensional pattern classification study. Neuroimage 41:277–285

Fink M, Akimova E, Spindelegger C, Hahn A, Lanzenberger R, Kasper S (2009) Social anxiety disorder: epidemiology, biology and treatment. Psychiatr Danub 21:533–542

Fouche JP, van Der Wee NJ, Roelofs K, Stein DJ (2013) Recent advances in the brain imaging of social anxiety disorder. Hum Psychopharmacol 28:102–105

Fox MD, Greicius M (2010) Clinical applications of resting state functional connectivity. Front Syst Neurosci 4:19

Fox MD, Snyder AZ, Vincent JL, Corbetta M, Van Essen DC, Raichle ME (2005) The human brain is intrinsically organized into dynamic, anticorrelated functional networks. Proc Natl Acad Sci USA 102:9673–9678

Fox MD, Zhang D, Snyder AZ, Raichle ME (2009) The global signal and observed anticorrelated resting state brain networks. J Neurophysiol 101:3270–3283

Friston KJ (2004) Functional integration in the brain. In: Human brain function, 2nd edn. Academic Press, San Diego pp 971–997

Frith U, Frith CD (2003) Development and neurophysiology of mentalizing. Philos Trans R Soc Lond B Biol Sci 358:459–473

Gentili C, Gobbini MI, Ricciardi E, Vanello N, Pietrini P, Haxby JV, Guazzelli M (2008) Differential modulation of neural activity throughout the distributed neural system for face perception in patients with Social Phobia and healthy subjects. Brain Res Bull 77:286–292

Gentili C, Ricciardi E, Gobbini MI, Santarelli MF, Haxby JV, Pietrini P, Guazzelli M (2009) Beyond amygdala: default mode network activity differs between patients with social phobia and healthy controls. Brain Res Bull 79:409–413

Goldin PR, Gross JJ (2010) Effects of mindfulness-based stress reduction (MBSR) on emotion regulation in social anxiety disorder. Emotion 10:83–91

Goldin PR, Manber-Ball T, Werner K, Heimberg R, Gross JJ (2009a) Neural mechanisms of cognitive reappraisal of negative self-beliefs in social anxiety disorder. Biol Psychiatry 66:1091–1099

Goldin PR, Manber T, Hakimi S, Canli T, Gross JJ (2009b) Neural bases of social anxiety disorder: emotional reactivity and cognitive regulation during social and physical threat. Arch Gen Psychiatry 66:170–180

Golland P, Fischl B (2003) Permutation tests for classification: towards statistical significance in image-based studies. Inf Process Med Imaging 18:330–341

Greicius M (2008) Resting-state functional connectivity in neuropsychiatric disorders. Curr Opin Neurol 21:424

Gross-Isseroff R, Kushnir T, Hermesh H, Marom S, Weizman A, Manor D (2010) Alteration learning in social anxiety disorder: an fMRI study. World J Biol Psychiatry 11:352–356

Guo WB, Liu F, Xue ZM, Yu Y, Ma CQ, Tan CL, Sun XL, Chen JD, Liu ZN, Xiao CQ, Chen HF, Zhao JP (2011) Abnormal neural activities in first-episode, treatment-naive, short-illness-duration, and treatment-response patients with major depressive disorder: a resting-state fMRI study. J Affect Disord 135:326–331

Guo W, Liu F, Xue Z, Gao K, Liu Z, Xiao C, Chen H, Zhao J (2013) Abnormal resting-state cerebellar-cerebral functional connectivity in treatment-resistant depression and treatment sensitive depression. Prog Neuropsychopharmacol Biol Psychiatry 44:51–57

Guyon I, Weston J, Barnhill S, Vapnik V (2002) Gene selection for cancer classification using support vector machines. Mach Learn 46:389–422

Hagmann P, Cammoun L, Gigandet X, Meuli R, Honey CJ, Wedeen VJ, Sporns O (2008) Mapping the structural core of human cerebral cortex. PLoS Biol 6:e159

Hahn A, Stein P, Windischberger C, Weissenbacher A, Spindelegger C, Moser E, Kasper S, Lanzenberger R (2011) Reduced resting-state functional connectivity between amygdala and orbitofrontal cortex in social anxiety disorder. Neuroimage 56:881–889

Haker A, Aderka IM, Marom S, Hermesh H, Gilboa-Schechtman E (2013) Impression formation and revision in social anxiety disorder. J Anxiety Disord

Hattingh CJ, Ipser J, Tromp SA, Syal S, Lochner C, Brooks SJ, Stein DJ (2012) Functional magnetic resonance imaging during emotion recognition in social anxiety disorder: an activation likelihood meta-analysis. Frontiers Hum Neurosci 6:347

Hayasaka S, Laurienti PJ (2010) Comparison of characteristics between region-and voxel-based network analyses in resting-state fMRI data. Neuroimage 50:499–508

Huang CL, Chen MC, Wang CJ (2007) Credit scoring with a data mining approach based on support vector machines. Expert Syst Appl 33:847–856

Jefferys D (1997) Social phobia. The most common anxiety disorder. Aust Fam Physician 26(1061):1064

Jiang T (2013) Brainnetome: a new -ome to understand the brain and its disorders. Neuroimage 80:263–272

Kilts CD, Kelsey JE, Knight B, Ely TD, Bowman FD, Gross RE, Selvig A, Gordon A, Newport DJ, Nemeroff CB (2006) The neural correlates of social anxiety disorder and response to pharmacotherapy. Neuropsychopharmacology 31:2243–2253

Kriegeskorte N, Simmons WK, Bellgowan PS, Baker CI (2009) Circular analysis in systems neuroscience: the dangers of double dipping. Nat Neurosci 12:535–540

Liao W, Chen H, Feng Y, Mantini D, Gentili C, Pan Z, Ding J, Duan X, Qiu C, Lui S, Gong Q, Zhang W (2010a) Selective aberrant functional connectivity of resting state networks in social anxiety disorder. Neuroimage 52:1549–1558

Liao W, Zhang Z, Pan Z, Mantini D, Ding J, Duan X, Luo C, Lu G, Chen H (2010b) Altered functional connectivity and small-world in mesial temporal lobe epilepsy. PLoS ONE 5:e8525

Lindquist KA, Wager TD, Kober H, Bliss-Moreau E, Barrett LF (2012) The brain basis of emotion: a meta-analytic review. Behav Brain Sci 35:121–143

Liu Y, Yu C, Liang M, Li J, Tian L, Zhou Y, Qin W, Li K, Jiang T (2007) Whole brain functional connectivity in the early blind. Brain J Neurol 130:2085–2096

Liu Y, Liang M, Zhou Y, He Y, Hao Y, Song M, Yu C, Liu H, Liu Z, Jiang T (2008) Disrupted small-world networks in schizophrenia. Brain 131:945–961

Liu F, Guo W, Yu D, Gao Q, Gao K, Xue Z, Du H, Zhang J, Tan C, Liu Z, Zhao J, Chen H (2012a) Classification of different therapeutic responses of major depressive disorder with multivariate pattern analysis method based on structural MR scans. PLoS ONE 7:e40968

Liu F, Hu M, Wang S, Guo W, Zhao J, Li J, Xun G, Long Z, Zhang J, Wang Y, Zeng L, Gao Q, Wooderson SC, Chen J, Chen H (2012b) Abnormal regional spontaneous neural activity in first-episode, treatment-naive patients with late-life depression: a resting-state fMRI study. Prog Neuropsychopharmacol Biol Psychiatry 39:326–331

Luo C, Qiu C, Guo Z, Fang J, Li Q, Lei X, Xia Y, Lai Y, Gong Q, Zhou D, Yao D (2011) Disrupted functional brain connectivity in partial epilepsy: a resting-state fMRI study. PLoS ONE 7:e28196

Mayberg HS, Liotti M, Brannan SK, McGinnis S, Mahurin RK, Jerabek PA, Silva JA, Tekell JL, Martin CC, Lancaster JL, Fox PT (1999) Reciprocal limbic-cortical function and negative mood: converging PET findings in depression and normal sadness. Am J Psychiatry 156:675–682

Meier TB, Desphande AS, Vergun S, Nair VA, Song J, Biswal BB, Meyerand ME, Birn RM, Prabhakaran V (2012) Support vector machine classification and characterization of age-related reorganization of functional brain networks. Neuroimage 60:601–613

Milad MR, Rauch SL (2007) The role of the orbitofrontal cortex in anxiety disorders. Ann N Y Acad Sci 1121:546–561

Mitchell TM (1997) Machine learning, vol 45. McGraw Hill, Burr Ridge

Mourao-Miranda J, Bokde AL, Born C, Hampel H, Stetter M (2005) Classifying brain states and determining the discriminating activation patterns: Support Vector Machine on functional MRI data. Neuroimage 28:980–995

Murphy K, Birn RM, Handwerker DA, Jones TB, Bandettini PA (2009) The impact of global signal regression on resting state correlations: are anti-correlated networks introduced? Neuroimage 44:893–905

Nakao T, Sanematsu H, Yoshiura T, Togao O, Murayama K, Tomita M, Masuda Y, Kanba S (2011) fMRI of patients with social anxiety disorder during a social situation task. Neurosci Res 69:67–72

Norman KA, Polyn SM, Detre GJ, Haxby JV (2006) Beyond mind-reading: multi-voxel pattern analysis of fMRI data. Trends Cogn Sci 10:424–430

Ohayon MM, Schatzberg AF (2010) Social phobia and depression: prevalence and comorbidity. J Psychosom Res 68:235–243

Olson IR, Plotzker A, Ezzyat Y (2007) The enigmatic temporal pole: a review of findings on social and emotional processing. Brain 130:1718–1731

Pereira F, Mitchell T, Botvinick M (2009) Machine learning classifiers and fMRI: a tutorial overview. Neuroimage 45:S199–S209

Polosan M, Baciu M, Cousin E, Perrone M, Pichat C, Bougerol T (2011) An fMRI study of the social competition in healthy subjects. Brain Cogn 77:401–411

Power JD, Barnes KA, Snyder AZ, Schlaggar BL, Petersen SE (2012) Spurious but systematic correlations in functional connectivity MRI networks arise from subject motion. Neuroimage 59:2142–2154

Qiu C, Liao W, Ding J, Feng Y, Zhu C, Nie X, Zhang W, Chen H, Gong Q (2011) Regional homogeneity changes in social anxiety disorder: a resting-state fMRI study. Psychiatry Res 194:47–53

Raichle ME, MacLeod AM, Snyder AZ, Powers WJ, Gusnard DA, Shulman GL (2001) A default mode of brain function. Proc Natl Acad Sci USA 98:676–682

Saad ZS, Gotts SJ, Murphy K, Chen G, Jo HJ, Martin A, Cox RW (2012) Trouble at rest: how correlation patterns and group differences become distorted after global signal regression. Brain Connectivity 2:25–32

Satterthwaite TD, Wolf DH, Loughead J, Ruparel K, Elliott MA, Hakonarson H, Gur RC, Gur RE (2012) Impact of in-scanner head motion on multiple measures of functional connectivity: relevance for studies of neurodevelopment in youth. Neuroimage 60:623–632

Schmahmann JD (2010) The role of the cerebellum in cognition and emotion: personal reflections since 1982 on the dysmetria of thought hypothesis, and its historical evolution from theory to therapy. Neuropsychol Rev 20:236–260

Schölkopf B, Smola AJ (2001) Learning with kernels: Support vector machines, regularization, optimization, and beyond. MIT press, Cambridge

Shi F, Liu Y, Jiang T, Zhou Y, Zhu W, Jiang J, Liu H, Liu Z (2007) Regional homogeneity and anatomical parcellation for fMRI image classification: application to schizophrenia and normal controls. Med Image Comput Comput Assist Interv 10:136–143

Smith K (2012) Brain imaging: fMRI 2.0. Nature 484:24–26

Sorg C, Riedl V, Mühlau M, Calhoun VD, Eichele T, Läer L, Drzezga A, Förstl H, Kurz A, Zimmer C (2007) Selective changes of resting-state networks in individuals at risk for Alzheimer's disease. Proc Natl Acad Sci USA 104:18760–18765

Sporns O (2011) The human connectome: a complex network. Ann N Y Acad Sci 1224:109–125

Stein JF, Glickstein M (1992) Role of the cerebellum in visual guidance of movement. Physiol Rev 72:967–1017

Stein MB, Stein DJ (2008) Social anxiety disorder. The Lancet 371:1115–1125

Su L, Wang L, Chen F, Shen H, Li B, Hu D (2012) Sparse representation of brain aging: extracting covariance patterns from structural MRI. PLoS ONE 7:e36147

Syal S, Hattingh CJ, Fouche JP, Spottiswoode B, Carey PD, Lochner C, Stein DJ (2012) Grey matter abnormalities in social anxiety disorder: a pilot study. Metab Brain Dis 27:299–309

Talati A, Pantazatos SP, Schneier FR, Weissman MM, Hirsch J (2013) Gray matter abnormalities in social anxiety disorder: primary, replication, and specificity studies. Biol Psychiatry 73:75–84

Tang Y, Jiang W, Liao J, Wang W, Luo A (2013) Identifying individuals with antisocial personality disorder using resting-state FMRI. PLoS ONE 8:e60652

Tian L, Wang J, Yan C, He Y (2011) Hemisphere- and gender-related differences in small-world brain networks: a resting-state functional MRI study. Neuroimage 54:191–202

Tillfors M, Furmark T, Marteinsdottir I, Fischer H, Pissiota A, Langstrom B, Fredrikson M (2001) Cerebral blood flow in subjects with social phobia during stressful speaking tasks: a PET study. Am J Psychiatry 158:1220–1226

Tillfors M, Furmark T, Marteinsdottir I, Fredrikson M (2002) Cerebral blood flow during anticipation of public speaking in social phobia: a PET study. Biol Psychiatry 52:1113–1119

Tzourio-Mazoyer N, Landeau B, Papathanassiou D, Crivello F, Etard O, Delcroix N, Mazoyer B, Joliot M (2002) Automated anatomical labeling of activations in SPM using a macroscopic anatomical parcellation of the MNI MRI single-subject brain. Neuroimage 15:273–289

Uddin LQ, Menon V, Young CB, Ryali S, Chen T, Khouzam A, Minshew NJ, Hardan AY (2011) Multivariate searchlight classification of structural magnetic resonance imaging in children and adolescents with autism. Biol Psychiatry 70:833–841

Van Dijk KR, Sabuncu MR, Buckner RL (2012) The influence of head motion on intrinsic functional connectivity MRI. Neuroimage 59:431–438

Vapnik VN (1995) The nature of statistical learning theory. Springer, New York Inc

Wang J, Wang L, Zang Y, Yang H, Tang H, Gong Q, Chen Z, Zhu C, He Y (2009) Parcellation-dependent small-world brain functional networks: a resting-state fMRI study. Hum Brain Mapp 30:1511–1523

Wang L, Shen H, Tang F, Zang Y, Hu D (2012) Combined structural and resting-state functional MRI analysis of sexual dimorphism in the young adult human brain: an MVPA approach. Neuroimage 61:931–940

Warwick JM, Carey P, Jordaan GP, Dupont P, Stein DJ (2008) Resting brain perfusion in social anxiety disorder: a voxel-wise whole brain comparison with healthy control subjects. Prog Neuropsychopharmacol Biol Psychiatry 32:1251–1256

Wee CY, Yap PT, Li W, Denny K, Browndyke JN, Potter GG, Welsh-Bohmer KA, Wang L, Shen D (2011) Enriched white matter connectivity networks for accurate identification of MCI patients. Neuroimage 54:1812–1822

Wee CY, Yap PT, Zhang D, Wang L, Shen D (2013) Group-constrained sparse fMRI connectivity modeling for mild cognitive impairment identification. Brain Struct Funct. doi:10.1007/s00429-013-0524-8

Yu C, Liu Y, Li J, Zhou Y, Wang K, Tian L, Qin W, Jiang T, Li K (2008) Altered functional connectivity of primary visual cortex in early blindness. Hum Brain Mapp 29:533–543

Zahn R, Moll J, Krueger F, Huey ED, Garrido G, Grafman J (2007) Social concepts are represented in the superior anterior temporal cortex. Proc Natl Acad Sci USA 104:6430–6435

Zalesky A, Fornito A, Harding IH, Cocchi L, Yucel M, Pantelis C, Bullmore ET (2010) Whole-brain anatomical networks: does the choice of nodes matter? Neuroimage 50:970–983

Zhang D, Wang Y, Zhou L, Yuan H, Shen D (2011a) Multimodal classification of Alzheimer's disease and mild cognitive impairment. Neuroimage 55:856–867

Zhang J, Wang J, Wu Q, Kuang W, Huang X, He Y, Gong Q (2011b) Disrupted brain connectivity networks in drug-naive, first-episode major depressive disorder. Biol Psychiatry 70:334–342

Zhang Z, Liao W, Chen H, Mantini D, Ding JR, Xu Q, Wang Z, Yuan C, Chen G, Jiao Q, Lu G (2011c) Altered functional-structural coupling of large-scale brain networks in idiopathic generalized epilepsy. Brain 134:2912–2928

Zhou B, Liu Y, Zhang Z, An N, Yao H, Wang P, Wang L, Zhang X, Jiang T (2013) Impaired functional connectivity of the thalamus in Alzheimer's disease and mild cognitive impairment: a resting-state fMRI study. Curr Alzheimer Res 10:754–766

Zhu CZ, Zang YF, Cao QJ, Yan CG, He Y, Jiang TZ, Sui MQ, Wang YF (2008) Fisher discriminative analysis of resting-state brain function for attention-deficit/hyperactivity disorder. Neuroimage 40:110–120